Available online at www.sciencedirect.com
SCIENCE DIRECT®
PERGAMON
International Journal of Heat and Mass Transfer 47 (2004) 63–74
International Journal of HEAT and MASS TRANSFER
www.elsevier.com/locate/ijhmt

Estimation of the nucleation probability in emulsions

S. Gibout *, M. Strub, J.P. Dumas

Laboratoire de Thermodynamique Énergétique et Procédés, Avenue de l'Université, BP 1155, 64013 Pau Cedex, France

Received 20 November 2001; received in revised form 17 June 2003

Abstract

A new method of determination of the nucleation probability of undercooled liquid dispersed within an emulsion is presented. The nucleation probability is a nonlinear function of the temperature depending on two parameters acting very differently. The aim of this paper is to present a method to determine these parameters by an inverse analysis of the heat transfer during the cooling of the emulsion. Information about the precision of the identification is also presented.

Keywords: Undercooling; Inverse problem; Numerical analysis; Nucleation probability

1. Introduction

The undercooling phenomenon is characterized by the persistence in liquid state of a material below its melting point T_F. If the crystallization occurs at temperature T, we can define the *undercooling* as being $\Delta T = T_F - T$.

It is well known that the main parameter which affects ΔT is the volume. ΔT increases when the size of the sample decreases. For example, for water ΔT is 14 K for a few cm^3, and about 38 K for a few μm^3.

Statistical studies [1], worked out on a large number of droplets (in an emulsion for example), evidence the stochastic character of the metastability breakdown. At constant temperature T, all droplets do not crystallize at the same time or during a steady cooling the crystallizations occur at different temperatures. Thus, for an isolated sample at a temperature T lower than T_F, we can only define the probability $J(T)$ of crystallization by unit of time. Nucleation theories [2,3] give this function as:

$$J(T) = A \cdot \exp\left(-\frac{B}{T \cdot (T - T_F)^2}\right) \quad \text{for } T < T_F \qquad (1)$$

where A (s^{-1}) and B (K^3) are constants. For convenience, we can widen the definition of $J(T)$ by putting $J(T) = 0$ for $T \geqslant T_F$.

The coefficient B is characteristic of the undercooled substance (molar volume of the crystal, interfacial tension liquid-crystal) whereas A depends on the volume of the crystal [1,2].

The function $J(T)$ is strongly nonlinear: its value remains very close to zero for a wide range of temperatures below T_F and then increases very quickly when T decreases (Fig. 1).

The function $J(T)$ has been determined by differential scanning calorimetry (DSC) for certain emulsions. For example, Fig. 1 represents the function $J(T)$ for an hexadecane emulsion within water [4]. However, this method is time consuming and requires very coercive experimental conditions. So, we attempted to develop a method and the related instrumentation allowing the determination of A and B by an inverse method requiring only measurements of the temperature of the sample during a steady cooling.

2. Direct problem

2.1. Hypothesis

The sample holder (Fig. 2) is a hollow cylinder, containing an emulsion, whose inner radius R is small

* Corresponding author.
E-mail addresses: stephane.gibout@univ-pau.fr (S. Gibout), michel.strub@univ-pau.fr (M. Strub), jean-pierre.dumas@univ-pau.fr (J.P. Dumas).

0017-9310/$ - see front matter
doi:10.1016/S0017-9310(03)00384-3

Nomenclature

A	pre-exponential coefficient of $J(T)$
B	exponential coefficient of $J(T)$
C	specific heat capacity of the sample
$\mathbb{D}$	matrix of diagonal terms of $\mathbb{X}^t \cdot \mathbb{X}$ ($n_p \times n_p$ matrix)
$\boldsymbol{e}$	error vector $\boldsymbol{e} = \boldsymbol{T} - \boldsymbol{Y}$
$J(T)$	probability of crystallization
J_P	first auxiliary parameter to identify
J'_P	second auxiliary parameter to identify
L	apparent latent heat of fusion of the sample
L_F	latent heat of fusion of the dispersed phase
$\boldsymbol{p}$	parameter vector ($n_p \times 1$ vector)
R	radius of the cylinder
S	criteria
T	temperature (general notation)
$\boldsymbol{T}(\boldsymbol{p})$	temperature response of the model ($n_m \times 1$ vector)
T_F	melting temperature
T_P	auxiliary temperature used in definitions of J_P and J'_P
$\mathbb{X}$	sensitivity matrix ($n_m \times n_p$ matrix)
$\boldsymbol{Y}$	experimental data ($n_m \times 1$ vector)

Greek symbols

δ	scalar parameter
λ	thermal conductivity
φ	crystallized fraction
ρ	density of the sample
σ	standard deviation
θ	discretized temperature

Subscripts

L	liquid state of the dispersed droplets
S	crystallized state of the dispersed droplets
∞	cooling fluid

Superscripts

k	iteration number
t	matrix transposition
$\sim$	quantity relative to the solution of the identification

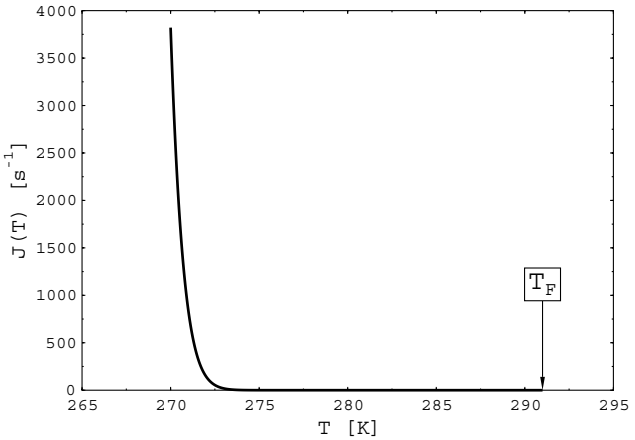

Fig. 1. Probability of crystallization of dispersed droplets.

with regard to its length. Some experimental results [5] have shown that the temperatures are axisymmetrical. So we consider an one-dimensional transient heat transfer model. For time $t \geqslant 0$ and position $0 \leqslant r \leqslant R$, the state of the sample is characterized by its temperature $T(r,t)$ and its crystallized fraction $\varphi(r,t)$, which is the proportion of droplets already transformed.

A previous study [6] evidenced a boundary value of the global heat transfer coefficient between the sample and the cooling fluid. This value is between 100 and 200 $\mathrm{W\,m^{-2}\,K^{-1}}$ according to the experimental conditions. It has been demonstrated that beyond this limit, the thermal transfers do not depend anymore on the value of this coefficient. In our experimental device, the circulation of the cooling fluid around the cell has been designed to have a higher heat transfer coefficient with the external interface. Several tests [7] realized with a characterized substance (glycerol) have shown that the heat transfer coefficient is higher than 500 $\mathrm{W\,m^{-2}\,K^{-1}}$. So, we shall use an imposed temperature as boundary condition.

The experimental conditions are always chosen in a way that only the dispersed phase crystallizes during the cooling, the emulsifying medium remaining in the liquid state. For the concerned emulsions, the dispersed

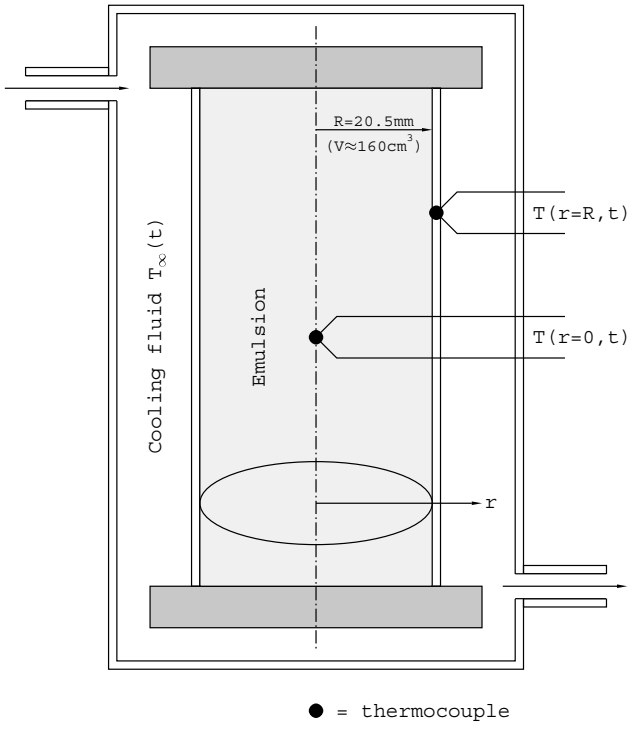

Fig. 2. Experimental device.

droplets are small enough to consider the emulsion as homogeneous, and all physical quantities are relative to this homogeneous phase. Further the studied emulsions are supposed to be viscous enough to neglect the convection phenomenon.

The thermal conductivity λ and the specific heat C are supposed to be constant with regard to the temperature. However, these properties vary as the dispersed phase is solid (λ_S and C_S), liquid (λ_L and C_L) or in an intermediate state characterized by $0 < \varphi < 1$. We have chosen a linear law [7] and we will use the following relations:

$$\begin{cases} C(\varphi) = C_L + (C_S - C_L) \cdot \varphi \\ \lambda(\varphi) = \lambda_L + (\lambda_S - \lambda_L) \cdot \varphi \end{cases} \quad (2)$$

Comparisons between simulations and measurements showed the validity of these relations for our model. [6].

Most of the properties of the emulsion depend on Φ which is the mass fraction of the dispersed substance (ratio of the mass of the dispersed liquid to the total mass of the emulsion). For a given Φ, all these properties are supposed to be constant.

2.2. Mathematical model

While supposing the previous assumptions, we use the following energy equation:

$$\rho \cdot C(r,t) \cdot \frac{\partial T(r,t)}{\partial t} = \frac{1}{r} \cdot \frac{\partial}{\partial r}\left(r \cdot \lambda(r,t) \cdot \frac{\partial T(r,t)}{\partial r} \right) + \dot{q}(r,t) \quad (3)$$

The heat source term $\dot{q}(r,t)$ is different from zero only when the crystallization of the undercooled droplets occurs i.e. when $J(T(r,t)) > 0$ and $\varphi(r,t) < 1$.

Let us consider a large number N of droplets per unit volume of dispersion. Initially, all droplets are liquid and we impose a temperature lower than T_F. If at an instant $t > 0$, we have $n(r,t)$ droplets in a solid state per unit volume, a number $dn(r,t)$ of the $N - n(r,t)$ remaining liquid droplets will crystallize between t and $t + dt$. This number is proportional to the remaining number of liquid droplets and to the probability of crystallization by unit of time $J(T)$. So, we can write:

$$dn(r,t) = (N - n(r,t)) \cdot J(T(r,t)) \cdot dt \quad (4)$$

Dividing by N and defining the proportion of crystallized droplets as $\varphi(r,t) = n(r,t)/N$, we get the Eq. (5) that describes the kinetics of crystallization:

$$\frac{d\varphi(r,t)}{dt} = (1 - \varphi(r,t)) \cdot J(T(r,t)) \quad (5)$$

To express the heat source term $\dot{q}(r,t)$, we suppose that the release of heat due to the crystallization is instantaneous for each drop. Under the hypothesis of

homogeneity, we assume furthermore that the sample has an apparent latent heat L ($\mathrm{J\,kg^{-1}}$), which is, for example, directly accessible to a calorimetric measurement. The dispersed phase being the only one concerned by a phase change, we have $L = \Phi \cdot L_F$ where L_F is the latent heat of the dispersed phase. Then we obtain:

$$\dot{q}(r,t) = \rho \cdot L \cdot \frac{\mathrm{d}\varphi(r,t)}{\mathrm{d}t} \tag{6}$$

As we mentioned previously, the boundary condition for $r = R$ is

$$T(r,t) = T_\infty(t) \quad \text{at } r = R, \ t > 0 \tag{7}$$

where $T_\infty(t)$ is the fluid temperature outside of the cell, depending on time. The condition of symmetry in $r = 0$ imposes:

$$\frac{\partial T(r,t)}{\partial r} = 0 \quad \text{at } r = 0, \ t > 0 \tag{8}$$

Initial conditions are:

$$\begin{cases} T(r,t) = T_\infty(0) > T_F & \text{for } 0 \leqslant r \leqslant R, \ t = 0 \\ \varphi(r,t) = 0 & \text{for } 0 \leqslant r \leqslant R, \ t = 0 \end{cases} \tag{9}$$

$T_\infty(0)$ being greater than T_F, all droplets are initially in the liquid state.

2.3. Numerical algorithm for solving the direct problem

The domain is divided into annular cells, in which both temperature and crystallized fraction are supposed to be uniform (Fig. 3). We notice θ_m^i and φ_m^i respectively the temperature and the crystallized fraction in the node $m = 1, 2, \ldots, M$ and at the time $i = 1, 2, \ldots, I$.

Because of the nonlinearity introduced by the term source, we opted for a fully explicit scheme. Preliminary attempts, using an implicit or semi-implicit scheme, did not allow us to obtain the convergence of the calculations of fields with a reasonable number of time steps. So, the explicit method remains faster, in spite of the constraint on Δt and Δr imposed by the condition of stability:

$$\frac{\Delta t}{(\Delta r)^2} \leqslant \frac{\rho \cdot \min(C_L, C_S)}{4 \cdot \max(\lambda_L, \lambda_S)} \tag{10}$$

In practice, Δr is imposed by the user while Δt is calculated in order to satisfy the above condition.

Fig. 4 shows a result of simulation giving the axial temperature versus time for an emulsion [6] ($T_F = 291$ K, $A = 1.8 \times 10^{10}$ $\mathrm{s^{-1}}$, $B = 1.8 \times 10^6$ $\mathrm{K^3}$, $\Phi = 0.5$). This curve will be chosen as the reference for all the analyses of the behaviour of the algorithm.

The cooling can be decomposed into three successive parts: the first one ($t < 1.7$ h) corresponds to a steady cooling where the dispersed phase remains in the liquid state ($\varphi = 0$). At $t = 1.7$ h, the crystallizations begin ($\varphi > 0$), leading to a release of energy within the emulsion. It results a stabilisation of the temperature around

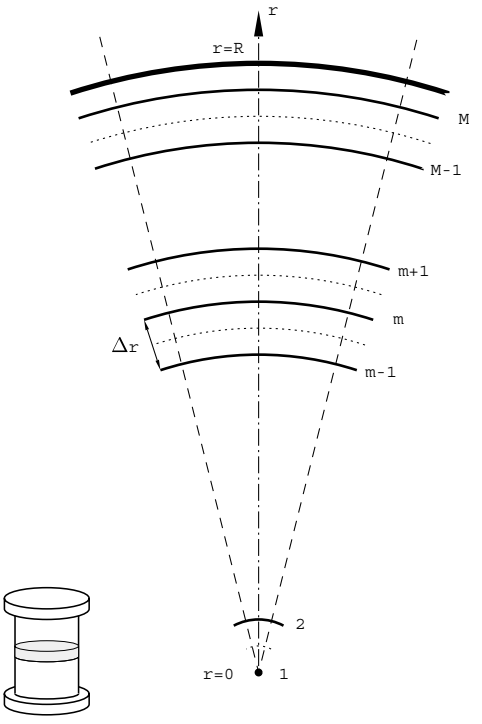

Fig. 3. Meshing of the domain.

$T^* \approx 278$ K during about 2 h. The undercooling $\Delta T = T_F - T^*$ is around 13 K. At $t = 3.6$ h, the last liquid droplet crystallizes and the temperature rapidly falls.

The temperature stabilisation during the cooling can be explained by an self-regulation phenomenon: when the temperature reaches a value where $J(T)$ is different from zero (Fig. 1), there are some crystallizations inducing a release of heat which would increase the temperature. But, if the temperature is increased, the probability of crystallization $J(T)$ decreases and the crystallization of the neighbouring droplets becomes less probable. It is necessary to wait for a further local cooling before additional crystallizations occur.

We also can see a consequence of this self-regulation on the Fig. 4, the major part of the crystallizations occurring at the end of the temperature stabilisation [5,6].

Fig. 5 shows the axial temperature evolution for several values of A and B. We notice that the effect of a variation of $\pm 10\%$ on B strongly modifies the evolution of the axial temperature, while a variation of 40% on A has a weaker influence. This weak influence will have consequences on the estimation problem.

3. Inverse problem

The inverse problem presented in this paper consists of the determination of the nucleation probability $J(T)$. The mathematical expression of $J(T)$ being known (Eq.

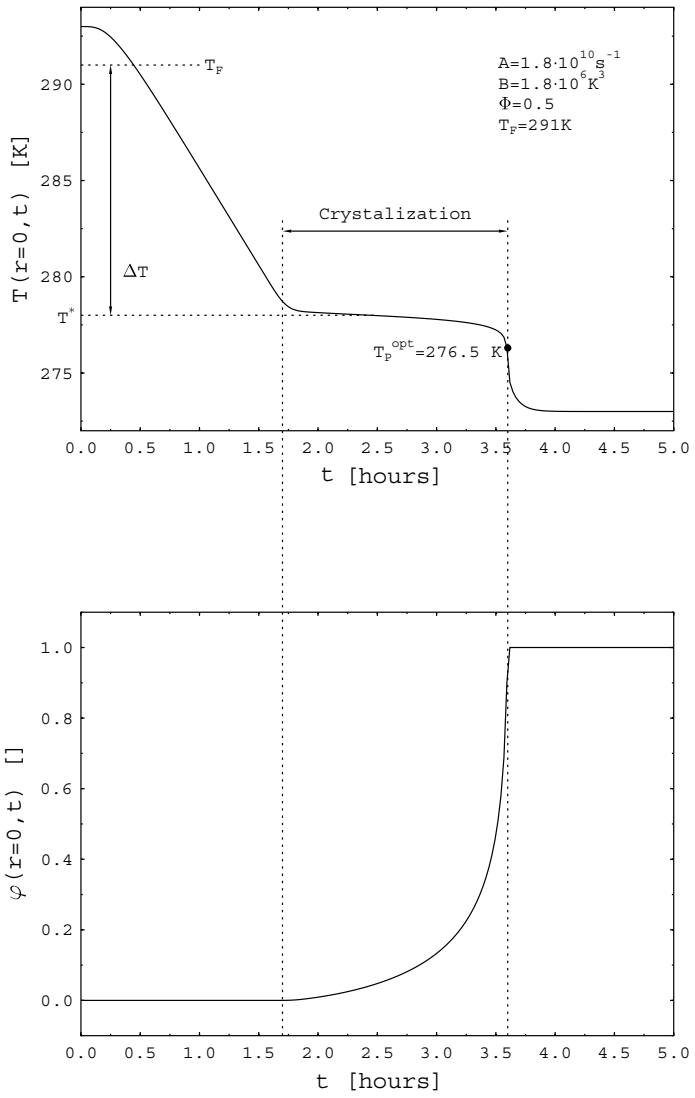

Fig. 4. Typical forms of $T(r=0,t)$ and $\varphi(r=0,t)$ during cooling.

(1)), the inverse problem is equivalent to finding out two parameters, whose choice will be justified.

The inversion is made from the temperatures measured on the axis of the cylinder ($r=0$) with regular time steps during the cooling. As the condition of symmetry imposes $\partial T(r,t)/\partial r|_{r=0}=0$, this location minimizes the errors of measurement induced by a bad centering of the sensor. Several tests also showed that this position reduces the effect of the measurement noise on the solution [7].

3.1. Estimation procedure

The method is derived from the Gauss's method and is based on the Levenberg–Marquardt approach [8]. This formulation allows to take advantage of both steepest descent and Newton's methods. Let's remind that the steepest descent method does not require a good initial guess but has a slow convergence. Inversely the Newton's method is fast but requires to be near the solution.

We note $\boldsymbol{p}=[p_1,\ldots,p_{n_p}]^t$ the vector of the n_p parameters to identify. The error vector $\boldsymbol{e}=[e_1,\ldots,e_{n_m}]^t$ contains the difference between the response of the model $\boldsymbol{T}=[T_1,\ldots,T_{n_m}]^t$ and the values of the n_m observed temperatures $\boldsymbol{Y}=[Y_1,\ldots,Y_{n_m}]^t$.

Find the solution of the inverse problem is equivalent to minimize the following sum of squares function:

$$S(\boldsymbol{p})=\boldsymbol{e}^t(\boldsymbol{p})\cdot\boldsymbol{e}(\boldsymbol{p})=\sum_{i=1}^{n_m}(e_i^2)\quad\text{where }\boldsymbol{e}(\boldsymbol{p})=\boldsymbol{T}(\boldsymbol{p})-\boldsymbol{Y} \tag{11}$$

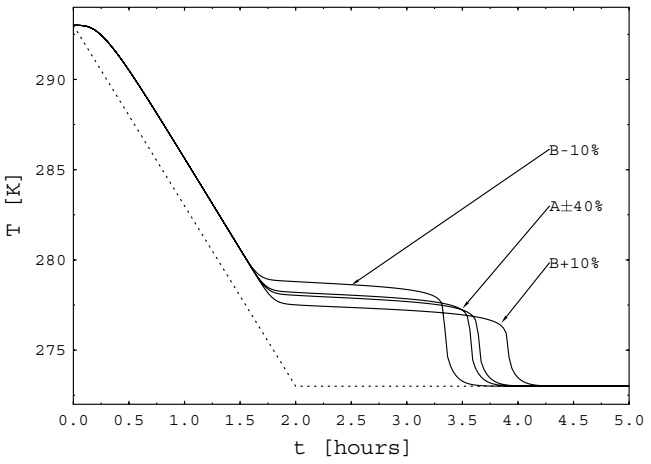

Fig. 5. Influence of A and B on the field of temperature.

The problem being nonlinear, an iterative method is used: from an initial guess $\boldsymbol{p}^{(0)}$, we build the series of the $\boldsymbol{p}^{(k)}$ (where k is the iteration index) as globally $S^{(k+1)} < S^{(k)}$. The iterative equation comes from the Gauss method:

$$\boldsymbol{p}^{(k+1)} = \boldsymbol{p}^{(k)} - [\mathbb{X}^{t(k)} \cdot \mathbb{X}^{(k)} + \mathbb{U}^{(k)}]^{-1} \cdot [\mathbb{X}^{t(k)} \cdot \boldsymbol{e}^{(k)}] \tag{12}$$

The sensitivity matrix $\mathbb{X}$ and $\mathbb{U}$ are defined as follow:

$$\mathbb{X}^{(k)} = [x_{i,j}] \quad \text{with } x_{i,j} = \left.\frac{\partial e_i^{(k)}}{\partial p_j^{(k)}}\right|_{i=1,\ldots,n_m,\ \ j=1,\ldots,n_p} \tag{13}$$

and

$$\mathbb{U}^{(k)} = \delta \cdot \frac{S(\boldsymbol{p}^{(k)})}{S(\boldsymbol{p}^{(0)})} \cdot \mathbb{D}^{(k)} \tag{14}$$

where $\mathbb{D}$ is the matrix of diagonal terms of $\mathbb{X}^t \cdot \mathbb{X}$. As $\mathbb{D}$ is defined from $\mathbb{X}$, the identification problem becomes invariant under scale changes in the parameters [8,10].

With this algorithm, the search direction is continuously updated by the intermediary of $\mathbb{U}$, according to the value of $S(\boldsymbol{p})$. Contrary to the Levenberg–Marquardt's method [8,10], we do not impose a "back-tracking" when the criterion does not decrease during an iteration.

At the beginning of the identification, the direction is close to the steepest descent one. During the iterative resolution, this direction progressively comes closer to the direction given by the Newton method. With this approach, the success of identification is not too much dependent on the initial guess (steepest descent), while the convergence is remaining fast (Newton).

During the first iterations (far from the solution), the matrix $\mathbb{X}^t \cdot \mathbb{X}$ is generally ill-conditioned and its inversion gives incorrect result leading to a wrong search direction. Then the matrix $\mathbb{U}^{(k)}$ allows the term $\mathbb{X}^t \cdot \mathbb{X} + \mathbb{U}^{(k)}$ to be a well-conditioned matrix. In the neighbourhood of the solution the matrix $\mathbb{U}^{(k)}$ vanishes because $S(\boldsymbol{p}^{(k)})$ tends to zero, meanwhile the matrix $\mathbb{X}^t \cdot \mathbb{X}$ becomes well-conditioned.

The coefficient δ is a positive scalar that is chosen according to the initial conditioning of the $\mathbb{X}^t \cdot \mathbb{X}$ matrix [7]. This coefficient defines the initial search direction: the more difficult is the case, the more δ must be high, the research direction approaching the steepest descent one.

3.2. Sensitivity coefficients calculus

From the definition of the error vector $\boldsymbol{e} = \boldsymbol{T}(\boldsymbol{p}) - \boldsymbol{Y}$, we can express $\mathbb{X}$ according to $\boldsymbol{T}(\boldsymbol{p})$, $\boldsymbol{Y}$ being independent from parameters:

$$\frac{\partial e_i}{\partial p_j} = \frac{\partial T_i}{\partial p_j} \quad \text{for } i = 1, \ldots, n_m \text{ and } j = 1, \ldots, n_p \tag{15}$$

We can differentiate the equations of the direct model with regard to each parameter. The calculation of sensitivity coefficients also requires the calculation of derivatives of φ with regard to each parameter.

In practice, calculus are made on the finite difference version of these equations. The resulting equations can be found in the Appendix B.

3.3. Choice of the parameters to be identified

The inverse method previously exposed is a general one. To apply it to our particular problem of identification, we must choose parameters that we want to find out.

In a first time, we have tried to find out A and B directly, putting $\boldsymbol{p} = [A, B]^t$. As we describe previously (Section 2.3 and Fig. 5), these two parameters have very

different effects. Consequently, the resulting sensitivity matrix $\mathbb{X}$ is unbalanced leading to a ill-conditioned matrix $\mathbb{X}^t \cdot \mathbb{X}$. In these conditions the algorithm cannot converge to the solution, even with the additional term $\mathbb{U}$.

To outline this difficulty, we introduce a temperature T_P and choose to put $\boldsymbol{p} = [J_P, J'_P]^t$ with:

$$J_P = J(T_P) = A \cdot \exp\left(-\frac{B}{T_P \cdot (T_P - T_F)^2} \right) > 0 \qquad (16)$$

and

$$J'_P = \left.\frac{\partial J(T)}{\partial T}\right|_{T=T_P} = J(T_P) \cdot B \cdot \frac{3 \cdot T_P - T_F}{T_P^2 \cdot (T_P - T_F)^3} < 0 \qquad (17)$$

With a good choice of T_P, the sensitivity coefficients with regard to J_P and J'_P have the same magnitude and identification can be made under better conditions.

Fig. 6 shows the required number of iteration to reach the solution for several values of T_P (based on simulated data, see Fig. 4). We can notice that the optimal choice of T_P corresponds approximately to the axial temperature at the moment when the crystallized fraction reaches $\varphi = 1$. The crystallized fraction being not measurable, we will notice that the previous condition is reached when the decrease of the axial temperature is the fastest. In the presented example, this optimal temperature is $T_P^{\text{opt}} \approx 276.3$ K.

For a T_P lower than T_P^{opt}, the convergence is slower but the solution is reached without exceeding the nominal value. If T_P is greater than T_P^{opt}, the solution is reached with exceeding or even cannot be reached.

When the solution is reached, values of A and B are calculated from the inverse formulas of J_P and J'_P:

$$A = J_P \cdot \exp\left[\frac{J'_P \cdot T_P \cdot (T_F - T_P)}{J_P \cdot (T_F - 3 \cdot T_P)} \right] \qquad (18)$$

and

$$B = \frac{J'_P \cdot T_P^2 \cdot (T_F - T_P)^3}{J_P \cdot (T_F - 3 \cdot T_P)} \qquad (19)$$

3.4. Precision of the identification

The analysis of an inverse problem shows that six different sources of errors can alter the precision of the solution [8]. In our work, we take into account the two most important sources:

- The measurement noise.
- The errors due to the known parameters of the model.

If we suppose that the measurement noise is additive and follows a normal distribution with zero mean value and constant standard deviation $\sigma_{\boldsymbol{Y}}$, we can use the following classical result [8]:

$$\text{cov}(\tilde{\boldsymbol{p}}) = \sigma_{\boldsymbol{Y}}^2 \cdot (\widetilde{\mathbb{X}}^t \cdot \widetilde{\mathbb{X}})^{-1} \qquad (20)$$

where $\tilde{\boldsymbol{p}}$ is the solution. The diagonal terms of $\text{cov}(\tilde{\boldsymbol{p}})$ are the standard deviations on the estimated parameters.

On the contrary the error on an input parameter has a systematic character and it is not possible to make a probability treatment. So, let us consider a known parameter π among ρ, λ_L, λ_S, C_L, C_S, T_F and L. A variation $\Delta\pi$ of π leads to a variation $\Delta\widetilde{\boldsymbol{T}}_\pi$ of the response $\widetilde{\boldsymbol{T}}$ of the model, inducing a variation $\Delta\tilde{\boldsymbol{e}}_\pi$ of $\tilde{\boldsymbol{e}}$. For small variation of $\Delta\pi$ around π, we can consider the model as linear and write:

$$\Delta\widetilde{\boldsymbol{T}}_\pi = \widetilde{\mathbb{X}}_\pi \cdot \Delta\pi \qquad (21)$$

where $\widetilde{\mathbb{X}}_\pi$ is the $n_m \times 1$ Sensitivity matrix of $\boldsymbol{T}$ with regard to the parameter π:

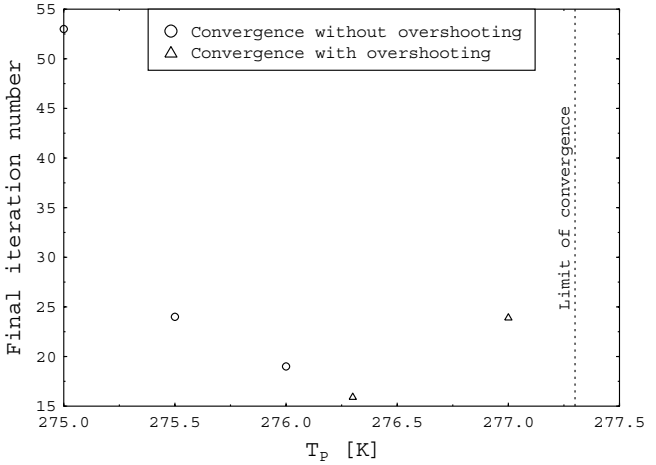

Fig. 6. Influence of T_P on the convergence.

$$\widetilde{\mathbb{X}}_\pi = \frac{\partial \boldsymbol{T}(\tilde{\boldsymbol{p}})}{\partial \pi} \tag{22}$$

(See Appendix B for details of the calculations of these matrix.)

In the neighbourhood of the acceptable solution $\tilde{\boldsymbol{p}}$, the value of the criterion is assumed to be very small, so we can consider that $S(\tilde{\boldsymbol{p}})/S(\boldsymbol{p}^{(0)})$ is close to zero, vanishing $\mathbb{U}^{(k)}$. With these hypotheses, any variation $\Delta\tilde{\boldsymbol{e}}_\pi$ of $\tilde{\boldsymbol{e}}$ induces a variation $\Delta\tilde{\boldsymbol{p}}_\pi$ of $\tilde{\boldsymbol{p}}$ about the solution. From Eq. (12) we can write:

$$\Delta\tilde{\boldsymbol{p}}_\pi = [\widetilde{\mathbb{X}}^t \cdot \mathbb{W} \cdot \widetilde{\mathbb{X}}]^{-1} \cdot [\widetilde{\mathbb{X}}^t \cdot \mathbb{W} \cdot \Delta\tilde{\boldsymbol{e}}_\pi] \tag{23}$$

where all values with a tilde are relative to the solution.

Thus, Eq. (23) becomes:

$$\Delta\tilde{\boldsymbol{p}}_\pi = [\widetilde{\mathbb{X}}^t \cdot \mathbb{W} \cdot \widetilde{\mathbb{X}}]^{-1} \cdot \widetilde{\mathbb{X}}^t \cdot \mathbb{W} \cdot \mathbb{X}_\pi \cdot \Delta\pi \tag{24}$$

In our particular case where we are using an intermediary couple of parameters J_P and J'_P to identify the values of A and B, the previous calculations gives us information about uncertainties on the parameters J_P and J'_P, which are to be transposed to A and B.

For small variations δJ_P and $\delta J'P$ around the solution, we can write:

$$\begin{bmatrix} \delta A \\ \delta B \end{bmatrix} = \begin{bmatrix} \frac{\partial A}{\partial J_P} & \frac{\partial A}{\partial J'_P} \\ \frac{\partial B}{\partial J_P} & \frac{\partial B}{\partial J'_P} \end{bmatrix} \cdot \begin{bmatrix} \delta J_P \\ \delta J'_P \end{bmatrix} \tag{25}$$

For systematic errors, We calculate ΔA and ΔB for each quantity π using the following equations:

$$\Delta A = \left|\frac{\partial A}{\partial J_P}\right| \cdot \Delta J_P + \left|\frac{\partial A}{\partial J'_P}\right| \cdot \Delta J'_P \tag{26}$$

and

$$\Delta B = \left|\frac{\partial B}{\partial J_P}\right| \cdot \Delta J_P + \left|\frac{\partial B}{\partial J'_P}\right| \cdot \Delta J'_P \tag{27}$$

where ΔJ_P and $\Delta J'_P$ are calculated from $\Delta\tilde{\boldsymbol{p}}_\pi$.

The variances $V(A)$ and $V(B)$ are calculated from the elements of the covariance matrix $\mathrm{cov}(\tilde{\boldsymbol{p}})$ (Eq. (20)) which is in our particular case:

$$\mathrm{cov}(\tilde{\boldsymbol{p}}) = \begin{bmatrix} V(J_P) & \mathrm{cov}(J_P, J'_P) \\ \mathrm{cov}(J_P, J'_P) & V(J'_P) \end{bmatrix} \tag{28}$$

While $V(aX + bY) = a^2 \cdot V(X) + b^2 \cdot V(Y) + 2ab \cdot \mathrm{cov}(X, Y)$, we obtain:

$$\begin{cases} V(A) = \left(\frac{\partial A}{\partial J_P}\right)^2 V(J_P) + \left(\frac{\partial A}{\partial J'_P}\right)^2 V(J'_P) \\ \qquad\quad +2\left(\frac{\partial A}{\partial J_P}\right)\left(\frac{\partial A}{\partial J'_P}\right)\mathrm{cov}(J_P, J'_P) \\ V(B) = \left(\frac{\partial B}{\partial J_P}\right)^2 V(J_P) + \left(\frac{\partial B}{\partial J'_P}\right)^2 V(J'_P) \\ \qquad\quad +2\left(\frac{\partial B}{\partial J_P}\right)\left(\frac{\partial B}{\partial J'_P}\right)\mathrm{cov}(J_P, J'_P) \end{cases} \tag{29}$$

The associated confidence intervals can be evaluated according to the classical property of the normal distribution ($\pm 2.58 \cdot \sigma$ for a 99% probability for example).

Finally, the global precision of the solution can be then estimated combining the $\Delta\tilde{\boldsymbol{p}}$ values for each parameter π and noise. We use the basic root-sum-square combinatorial Eq. [9]:

$$\Delta\tilde{\boldsymbol{p}}_j = \sqrt{\sum [(\Delta\tilde{\boldsymbol{p}}_\pi)_j]^2} \quad \text{for } j = 1, \ldots, n_p \tag{30}$$

4. Application

To validate our work, we have tested the method with experimental data. We chose an hexadecane emulsion already studied in the laboratory [4].

The physical properties have been determined either by a calorimetric method in the laboratory (C_L, C_S and L) or by an inverse method (λ_L and λ_S [7]). The different values are indicated in Table 1.

Initially, the temperature of the sample is homogeneous and equal to $T_\infty(0) = 300$ K. From $t = 0$, the temperature T_∞ of the outside fluid decreases linearly of $\beta = 10\ \mathrm{K\,hr^{-1}}$. After three hours, the temperature stabilizes at $T_{\min} = 270$ K till the end of the experiment (cf. Fig. 7).

$$T_\infty(t) = \begin{cases} -\beta \cdot t + T_\infty(0) & \text{when } T_\infty(t) \geqslant T_{\min} \\ T_{\min} & \text{later} \end{cases} \tag{31}$$

The measurements (Fig. 7) are made each minute during approximately 4.8 h ($n_m = 288$). Each measurement includes the axial temperature $T(r = 0, t)$ (for the inversion) and the temperature $T(r = R, t) = T_\infty(t)$ (for the boundary condition). Type K thermocouples are used.

The noise can be extracted from the measurement by applying a high pass filter to the original signal. The standard deviation can be then calculated and we find out $\sigma_Y \approx 3 \times 10^{-2}$ K.

Table 1
Thermophysical properties of the sample

$\rho = 932.5 \pm 0.5\ \mathrm{kg\,m^{-3}}$
$L = 108 \pm 1\ \mathrm{kJ\,kg^{-1}}$
$L_\mathrm{F} = 243 \pm 1\ \mathrm{kJ\,kg^{-1}}$
$\Phi = 0.44 \pm 0.01$
$\lambda_\mathrm{L} = 0.24 \pm 0.01\ \mathrm{W\,m^{-1}\,K^{-1}}$
$\lambda_\mathrm{S} = 0.38 \pm 0.01\ \mathrm{W\,m^{-1}\,K^{-1}}$
$C_\mathrm{L} = 2600 \pm 50\ \mathrm{J\,kg^{-1}\,K^{-1}}$
$C_\mathrm{S} = 2220 \pm 50\ \mathrm{J\,kg^{-1}\,K^{-1}}$
$T_\mathrm{F} = 291.3 \pm 0.1$ K

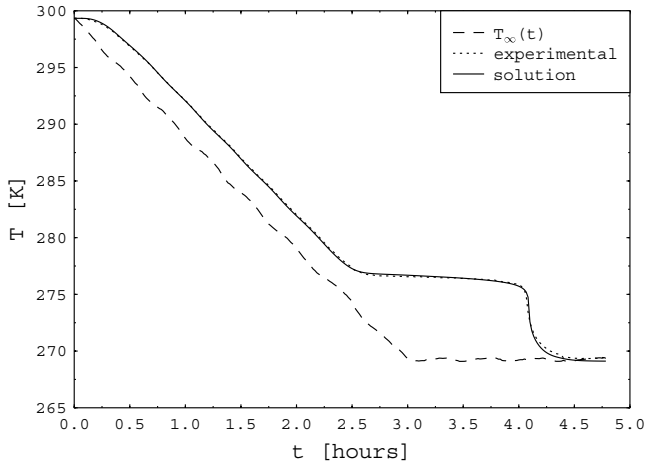

Fig. 7. Experimental data and solution.

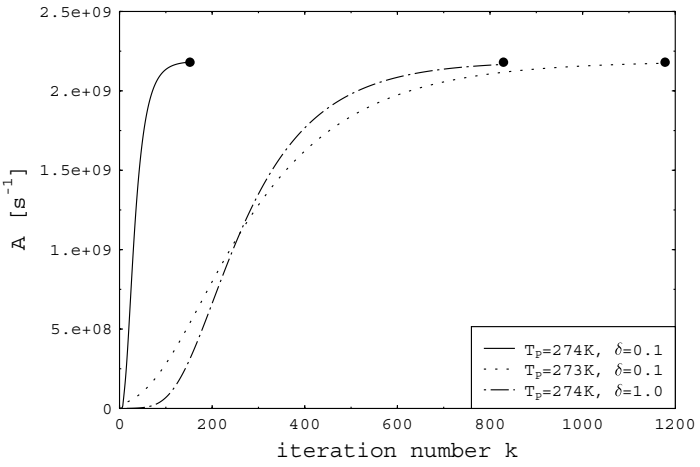

Fig. 8. Parameter A evolution.

Fig. 7 shows the experimental and calculated axial temperature based on the identified values.

Figs. 8 and 9 show results of inversions performed with several values of T_P and δ. According to the previous discussion, T_P^{opt} is about 274.5 K and T_P must be lower than 274.5 K in order to allow inversion in good conditions. These examples evidence the influence of T_P and δ on the convergence speed.

For the same value of T_P, the solution is reached after 152 iterations for $\delta = 0.1$, whereas 1178 iterations are necessary for $\delta = 1.0$. In the same way, for a constant $\delta = 0.1$, 829 iterations are necessary to reach the solution with $T_P = 273$ K, and only 152 with $T_P = 274$ K. For a T_P greater than $T_P^{\text{opt}} = 274.5$ K, the inversion cannot be performed. In every case we obtain the values $A = 2.18 \times 10^9$ s^{-1} and $B = 1.90 \times 10^6$ K^3.

Table 2 gives the influence of uncertainties of each input parameters on the solution according to (24).

We can notice that A is more influenced by the errors than B. The relative errors introduced on A are between 0.7% and 27.8% while they are lower than 0.2% on B. In spite of a very good precision on ρ and T_F, we notice that the corresponding uncertainties on A and B are not so small. In fact, if we consider the relative errors $\Delta A/A$ and $\Delta B/B$ for each input parameters with a constant $\Delta\pi/\pi$, the parameters L, ρ and T_F are the most influential on the precision of the solution.

Concerning the measurement noise influence, using Eq. (20), (26), and (27) we find $\sigma_A = 1.24 \times 10^4$ s^{-1} and $\sigma_B = 7.62 \times 10^1$ K^3 which can be neglected with regard to the other inaccuracies.

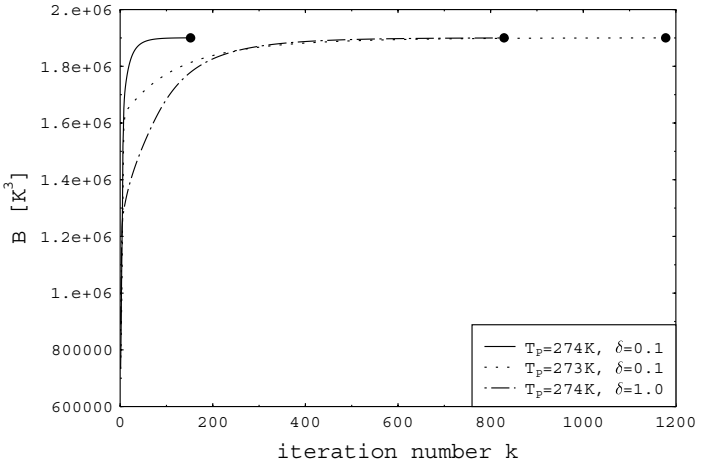

Fig. 9. Parameter B evolution.

Table 2
Influence of the input parameters uncertainties on the solution

π	$\Delta\pi$	$\Delta\pi/\pi(\%)$	ΔA (s^{-1})	$\Delta A/A(\%)$	ΔB (K^{-3})	$\Delta B/B(\%)$
λ_L	0.01	4.2	1.8×10^8	8.2	3.0×10^4	1.6
λ_S	0.01	2.6	5.9×10^8	27.8	3.8×10^4	2.0
C_L	50	1.9	3.6×10^8	16.4	8.8×10^3	0.5
C_S	50	2.3	2.9×10^8	13.2	6.1×10^3	0.3
L	1	0.9	5.4×10^8	24.6	2.7×10^4	1.4
ρ	0.5	5.4×10^{-2}	1.5×10^7	0.7	1.2×10^3	0.6
T_F	0.1	3.4×10^{-2}	4.1×10^8	18.6	3.7×10^4	1.9

Combining all the sources of error (Eq. (30)), we obtain finally $A = (2.2 \pm 0.9) \times 10^9$ s^{-1} and $B = (1.90 \pm 0.06) \times 10^6$ K^3.

If we compare the values of B obtained by DSC [4] i.e. $B = (1.9 \pm 0.1) \times 10^6$ K^3 and by our method, we notice a good agreement.

For the parameter A, the value determined by DSC is between 1.7×10^9 and 2.6×10^{11} s^{-1} with $A = 2.1 \times 10^{10}$ s^{-1} as the most probable value. Although these results are acceptable if we take uncertainties into account, this difference can be explained by the size of the droplets of emulsions [2].

On the contrary, the coefficient B being independent from the size of droplets, we understand that both determinations give the same value.

5. Conclusion

We finalized an inverse method of determination of the probability of crystallization in the case of droplets dispersed within an emulsion.

This method was validated by determining the parameters A and B of the nucleation probability $J(T)$ from experimental data. The influence of the uncertainties of the parameters on the solution was studied. We obtained for B a precise value ($\Delta B/B \approx 3\%$), in agreement with the previous determination by a calorimetric method.

The value of A is obtained with a less good precision ($\Delta A/A \approx 40\%$). Thus we still evidence the difficulty of identifying the parameter A, mainly because of its weak influence on the heat transfer during a cooling.

Appendix A. Finite difference equations

Let:

$$\Delta r = \frac{2 \cdot R}{2 \cdot M - 1}$$

$$\Delta t = \frac{T}{I - 1}$$

$$\theta_1^{i+1} = \theta_1^i + L \cdot \Delta t \cdot \frac{1}{C_1^i} \cdot (1 - \varphi_1^i) \cdot J(\theta_1^i) + 4 \cdot \frac{\Delta t}{\rho \cdot (\Delta r)^2} \cdot \frac{\lambda_1^i}{C_1^i} \cdot (\theta_2^i - \theta_1^i) \quad \text{(A.1)}$$

$$\theta_m^{i+1} = \theta_m^i + L\cdot\Delta t\cdot\frac{1}{C_1^i}\cdot(1-\varphi_1^i)\cdot J(\theta_1^i) + \frac{\Delta t}{\rho\cdot(\Delta r)^2}\cdot\frac{\lambda_m^i}{C_m^i}\cdot(\theta_{m+1}^i - 2\cdot\theta_m^i + \theta_{m-1}^i) + \frac{\Delta t}{\rho\cdot(\Delta r)^2}\cdot\frac{1}{2\cdot m-2}\cdot\frac{\lambda_m^i}{C_m^i}\cdot(\theta_{m+1}^i - \theta_{m-1}^i) \quad (A.2)$$

$$\theta_{M+1}^{i+1} = \theta_\infty^{i+1} \quad (A.3)$$

$$\varphi_m^{i+1} = \varphi_m^i + (1-\varphi_m^i)\cdot J(\theta_1^i)\cdot\Delta t \quad (A.4)$$

The boundaries conditions are:

$$\theta_m^1 = \theta_\infty^1 \quad \text{for } m = 1,\ldots,M$$

$$\theta_M^i = \theta_\infty^i \quad \text{for } i = 1,\ldots,I$$

$$\varphi_m^1 = 0 \quad \text{for } m = 1,\ldots,M$$

Appendix B. Sensitivity coefficients calculations

We first perform the derivation of the previous difference equations with regard to an arbitrary variable α. We set:

$$X_m^i = \frac{\partial\theta_m^i}{\partial\alpha}$$

$$Y_m^i = \frac{\partial\varphi_m^i}{\partial\alpha}$$

We obtain:

$$X_1^{i+1} = X_1^i + L\cdot\Delta t\cdot\frac{1}{C_1^i}\cdot D_1^i + L\cdot\Delta t\cdot\frac{F_1^i}{C_1^i}\cdot(1-\varphi_1^i)\cdot J(\theta_1^i) + 4\cdot\frac{\Delta t}{\rho\cdot(\Delta r)^2}\cdot\frac{\lambda_1^i}{C_1^i}\cdot(X_2^i - X_1^i) + 4\cdot\frac{\Delta t}{\rho\cdot(\Delta r)^2}\cdot\frac{E_1^i}{C_1^i}\cdot(\theta_2^i - \theta_1^i) \quad (B.1)$$

$$X_m^{i+1} = X_m^i + L\cdot\Delta t\cdot\frac{1}{C_m^i}\cdot D_m^i + L\cdot\Delta t\cdot\frac{F_m^i}{C_m^i}\cdot(1-\varphi_m^i)\cdot J(\theta_m^i) + \frac{\Delta t}{\rho\cdot(\Delta r)^2}\cdot\frac{\lambda_m^i}{C_m^i}\cdot(X_{m+1}^i - 2\cdot X_m^i + X_{m-1}^i) + \frac{\Delta t}{\rho\cdot(\Delta r)^2}\cdot\frac{1}{2\cdot m-2}\cdot\frac{\lambda_m^i}{C_m^i}\cdot(X_{m+1}^i - X_{m-1}^i) + \frac{\Delta t}{\rho\cdot(\Delta r)^2}\cdot\frac{E_m^i}{C_m^i}\cdot(\theta_{m+1}^i - 2\cdot\theta_m^i + \theta_{m-1}^i) + \frac{\Delta t}{\rho\cdot(\Delta r)^2}\cdot\frac{1}{2\cdot m-2}\cdot\frac{E_m^i}{C_m^i}\cdot(\theta_{m+1}^i - \theta_{m-1}^i) \quad (B.2)$$

$$X_{M+1}^{i+1} = 0 \quad (B.3)$$

$$Y_m^{i+1} = Y_m^i + D_m^i\cdot\Delta t \quad (B.4)$$

with:

$$D_m^i = Z_m^i\cdot(1-\varphi_m^i) - Y_m^i\cdot J(\theta_m^i)$$

$$Z_m^i = \frac{\partial}{\partial\alpha}[J(\theta_m^i)]$$

$$E_m^i = C_m^i\cdot\frac{\partial}{\partial\alpha}\left[\frac{K_m^i}{C_m^i}\right] = \frac{\partial K_m^i}{\partial\alpha} + K_m^i\cdot F_m^i$$

$$F_m^i = C_m^i\cdot\frac{\partial}{\partial\alpha}\left[\frac{1}{C_m^i}\right] = -\frac{1}{C_m^i}\cdot\frac{\partial C_m^i}{\partial\alpha}$$

Inversion algorithm and confidence interval calculation require to compute sensitivity coefficients for all variables. Table 3 indicates the expressions to be used according to the considered parameter.

$$F_1 = -\frac{C_S - C_L}{C_m^i}\cdot Y_m^i$$

$$F_2 = -\frac{1-\varphi_m^i - (C_S - C_L)\cdot Y_m^i}{C_m^i}$$

$$F_3 = -\frac{\varphi_m^i - (C_S - C_L)\cdot Y_m^i}{C_m^i}$$

$$E_1 = (\lambda_S - \lambda_L)\cdot Y_m^i + \lambda_m^i\cdot F_m^i$$

$$E_2 = 1 - \varphi_m^i + (\lambda_S - \lambda_L)\cdot Y_m^i + \lambda_m^i\cdot F_m^i$$

$$E_3 = \varphi_m^i + (\lambda_S - \lambda_L)\cdot Y_m^i + \lambda_m^i\cdot F_m^i$$

$$Z_1 = \exp\left(-\frac{B}{\theta_m^i\cdot(\theta_m^i - T_F)^2}\right)\cdot\left[\frac{\partial A}{\partial\alpha} - \frac{A}{\theta_m^i\cdot(\theta_m^i - T_F)^2}\cdot\frac{\partial B}{\partial\alpha} + \frac{A\cdot B\cdot(3\cdot\theta_m^i - T_F)}{(\theta_m^i)^2\cdot(\theta_m^i - T_F)^3}\cdot X_m^i\right]$$

$$Z_2 = J(\theta_m^i)\cdot B\cdot\frac{3\cdot\theta_m^i - T_F}{(\theta_m^i)^2\cdot(\theta_m^i - T_F)^3}\cdot X_m^i$$

$$Z_3 = J(\theta_m^i)\cdot\frac{X_m^i\cdot(3\cdot\theta_m^i - T_F) - 2\cdot\theta_m^i}{(\theta_m^i)^2\cdot(\theta_m^i - T_F)^3}$$

Finally, cases $\alpha = L$ and $\alpha = \rho$ require some additive terms. For $\alpha = L$, the following terms must be added to Eqs. (B.1) and (B.2):

$$X_1^{i+1} = \cdots + \frac{1}{C_1^i}\cdot\Delta t\cdot J(\theta_1^i)\cdot(1-\varphi_1^i)$$

$$X_m^{i+1} = \cdots + \frac{1}{C_m^i}\cdot\Delta t\cdot J(\theta_m^i)\cdot(1-\varphi_m^i)$$

For the case $\alpha = \rho$, the following terms must be added respectively to Eqs. (B.1) and (B.2):

$$X_1^i = \cdots - 4\cdot\frac{\lambda_1^i}{C_1^i}\cdot\frac{\Delta t}{\rho\cdot(\Delta r)^2}\cdot\frac{1}{\rho}\cdot(\theta_2^i - \theta_1^i)$$

Table 3
Sensitivity coefficients calculus cases

	J_P	J'_P	λ_L	λ_S	C_L	C_S	T_F	L	ρ
F_m^i	F_1	F_1	F_1	F_1	F_2	F_3	F_1	F_1	F_1
E_m^i	E_1	E_1	E_2	E_3	E_1	E_1	E_1	E_1	E_1
Z_m^i	Z_1	Z_1	Z_2	Z_2	Z_2	Z_2	Z_3	Z_2	Z_2

$$X_m^i = \cdots - \frac{\lambda_m^i}{C_m^i} \cdot \frac{\Delta t}{\rho \cdot (\Delta r)^2} \cdot \frac{1}{\rho} \cdot [\theta_{m+1}^i - 2 \cdot \theta_m^i + \theta_{m-1}^i] - \frac{1}{2 \cdot m - 2} \cdot \frac{\lambda_m^i}{C_m^i} \cdot \frac{\Delta t}{\rho \cdot (\Delta r)^2} \cdot \frac{1}{\rho} \cdot (\theta_{m+1}^i - \theta_{m-1}^i)$$

The boundaries conditions are:

$$X_m^1 = 0 \quad \text{and} \quad Y_m^1 = 0 \quad \text{for } m = 1, \ldots, M$$

$$X_M^i = 0 \quad \text{and} \quad Y_M^i = 0 \quad \text{for } i = 1, \ldots, I$$

References

[1] V.P. Skripov, Metastables Liquids, Wiley, New York, 1974.
[2] D. Turnbull, Phase Changes, Solid State Physics, Acad. Press Inc, 1956.
[3] H. Rasmussen, M.R. Appleby, G.L. Leedom, S.V. Babu, R.J. Naumann, Homogeneous nucleation kinetics, J Crystal Growth 64 (1983) 229–238.
[4] Y. Zéraouli, Étude thermique des transformations des émulsions concentrées: Application à la calorimétrie à balayage, Thèse de Doctorat, Université de Pau et des Pays de l'Adour, France, 1991.
[5] J.P. Dumas, Y. Zéraouli, M. Strub, M. Krichi, Models for the heat transfers during the transformations inside an emulsion: part I crystallization of the undercooled droplets, Int. J. Heat Mass Trans. 37 (1994) 737–746.
[6] M. Krichi, Étude thermique des transferts thermiques dans des systèmes dispersés subissant des transformations de phases, Thèse de Doctorat, Université de Pau et des Pays de l'Adour, France, 1992.
[7] Gibout S., Méthodes inverses de calcul appliquées à l'étude des transferts thermiques lors de la cristallisation de liquides dispersées surfondus, Thèse de Doctorat, Université de Pau et des Pays de l'Adour, France, 2001.
[8] J.V. Beck, K.J. Arnold, Parameter Estimation in Engineering and Science, Wiley, New York, 1977.
[9] R.J. Moffat, Contributions to the theory of single—sample uncertainty analysis, ASME J. Fluids Eng. 104 (1982) 250–260.
[10] E. Walter, L. Pronzato, Identification de modéles paramétriques à partir de données expérimentales, Masson, Paris, 1994.